WASHINGTON UNIVERSITY
DEPARTMENT OF PHYSICS
LABORATORY FOR ULTRASONICS
St. Louis, Missouri 63130

"Physical Principles of Ultrasonic Non-Destructive Evaluation of Advanced Composites"

Semiannual Progress Report: March 15, 1988 - September 14, 1988

NASA Grant Number: NSG-1601

Principal Investigator:

Dr. James G. Miller
Professor of Physics

The NASA Technical Officer for this grant is:

Dr. Joseph S. Heyman
NASA Langley Research Center
Hampton, Virginia

I. INTRODUCTION

In this Progress Report we will present results from our continued investigations into the use of ultrasonic measurement techniques for the detection and characerization of porosity. Previous Progress Reports (3/87 to 9/87 and 9/87 to 3/88) have described the use of such ultrasonic parameters as integrated polar backscatter and slope of attenuation as robust measurement tools for the interrogation of graphite/epoxy composites.

In Section II of this Progress Report we discuss our investigations into the effects that bleeder cloth impressions (left after the cure process) have on the capability of polar backscatter to interrogate volume effects such as porosity. In Section III we present some preliminary data regarding a comparison of phase-sensitive and phase-insensitive detection for materials characterization.

II. EFFECTS OF BLEEDER CLOTH IMPRESSIONS ON THE USE OF POLAR BACKSCATTER TO DETECT POROSITY

The potential of ultrasonic polar backscatter measurements for detecting and characterizing porosity in composite laminates has been investigated in a number of laboratories.[1-11] The objective of our study was to evaluate the influence of the nature of the composite's surface on such measurements. The deleterious effects of bleeder cloth impressions, previously noted by Bar-Cohen,[12] led to the hypothesis that the periodic surface features due to bleeder cloth impressions remaining after the cure process contribute significantly to the received backscattered signal, possibly masking the anisotropy of backscatter which is used to estimate porosity.

One measure of the anisotropy of polar backscatter is the integrated backscatter difference, defined in a pore-free region as the difference in decibels between the maximum and minimum integrated backscatter as a function of azimuthal angle. Figure 1 displays a typical polar backscatter anisotropy plot for a pore-free region of a uniaxial graphite/epoxy laminate. For ultrasound insonifying a planar composite laminate at a polar angle θ of 30°, backscatter is seen to be the strongest for insonification perpendicular to the fiber axes ($\phi = \pm 90°$). As illustrated in Figure 2 the anisotropy of polar backscatter can provide a useful index for quantitatively estimating the volume fraction of porosity.[6] Results from measurements on two regions of the same specimen are displayed to contrast the difference between "porous" and pore-free regions. Except for azimuthal angles $\phi \simeq \pm 90°$, strength of the received backscattered signal is significantly larger in the "porous" region than in the pore-free region, thus decreasing the anisotropy of polar backscatter. We therefore made use of the integrated backscatter difference to investigate the detrimental effects of the presence of bleeder cloth impressions on the

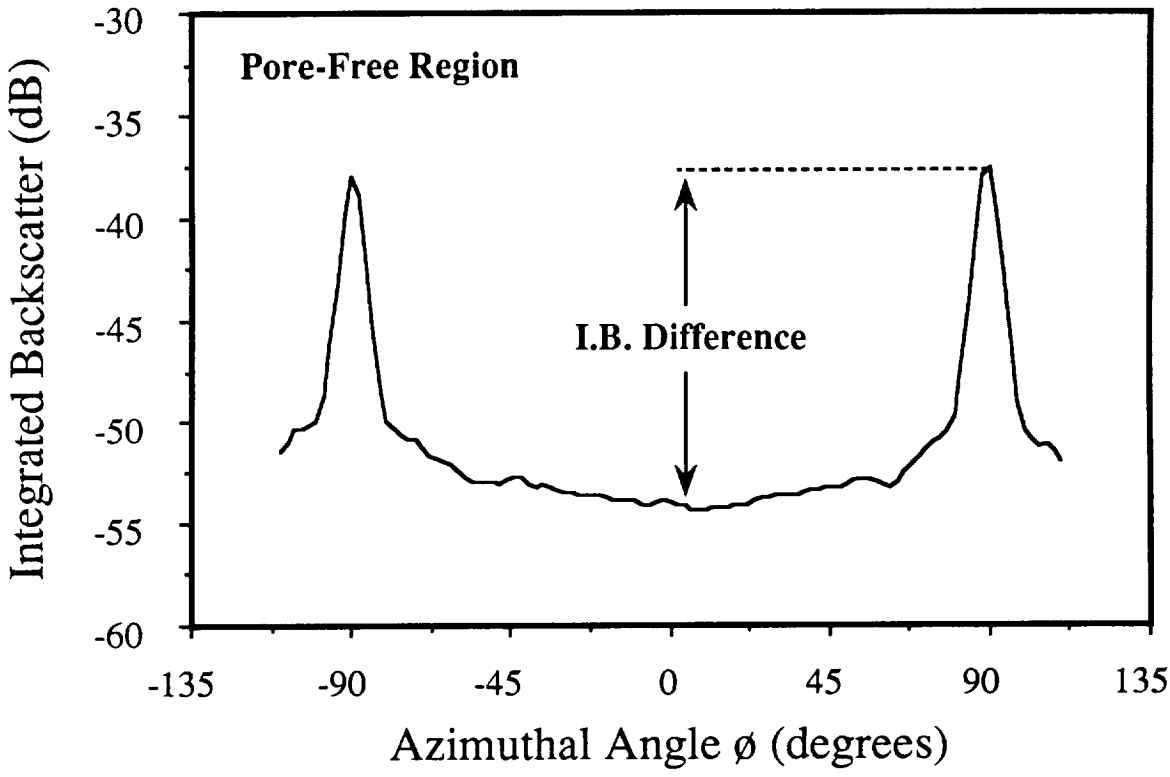

Figure 1: One measure of the anisotropy of polar backscatter is the integrated backscatter difference, defined in a pore-free region as the difference in dB between the maximum and minimum integrated backscatter as a function of azimuthal angle. Data were obtained from a pore-free region of a uniaxial graphite/epoxy composite.

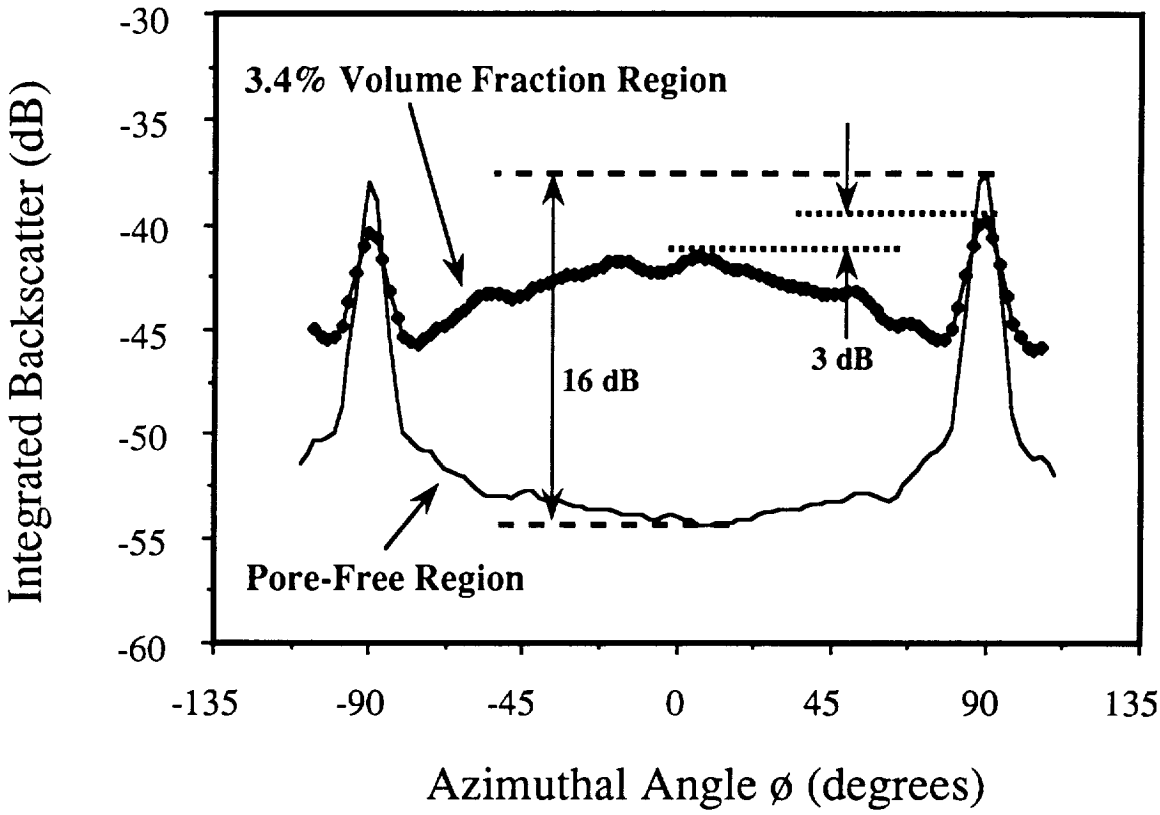

Figure 2: Results from two anisotropy scans: one in a pore-free region, the other in a "porous" region.

capability of ultrasonic polar backscatter imaging to detect and characterize porosity. The integrated backscatter difference was computed as the difference between measured values of integrated backscatter at the angles determined previously from the pore-free measurement, i.e., 90° and 0° for the case shown in Figure 2. (In the previous Progress Report from 9/87 to 3/88 we illustrated the advantages of averaging over a modest range of azimuthal angles to minimize background variations not attributable to porosity.)

EXPERIMENTAL METHODS

Sample Preparation

All the composites used in this study were fabricated at NASA Langley Research Center using #5208-T300 prepreg tape and a standard #234 TFP porous teflon coated fiberglass bleeder cloth. The effects of porosity were simulated by introducing hollow-carbon beads, having a distribution of diameters ranging from 5 to 150 microns, into a 16 ply uniaxial graphite-fiber/epoxy-matrix composite approximately 2 mm. thick. Measured amounts of hollow-carbon spherical inclusions were introduced between the 12th and 13th layers during the lay-up of a 12 by 16 inch laminate. The beads were dusted onto circular regions 2 inches in diameter at sites on a square grid with centers 4 inches apart. The sample was autoclaved and cured in an oven using a standard cure protocol. The 12 by 16 inch sample was cut into smaller samples (approximately 3.75" by 3.75") so that each contained a single zone of "porosity". In the present study we focused on samples of 2% and 3.4% volume fraction of "porosity".

Measurement Methods

Backscatter measurements were performed using a 10 MHz center frequency, 0.5 inch diameter, 4 inch focal length transducer employed in a pulse-echo mode. The transducer was oriented at a polar angle of 30° and at various azimuthal angles as described below. The polar backscatter technique, introduced by Bar-Cohen and Crane[1] and employed in several investigations reported from this[2,4-6] and other laboratories,[3,7,9] eliminates the strong surface reflections from the backscattered signal. Thus the specularly reflected signal is directed away from the transducer, which then receives only signals backscattered from variations in average material properties within the insonified volume of the specimen.

Data were collected over the frequency range 6 to 12 MHz in 0.04 MHz steps using the system shown in Figure 3. Backscatter was measured quantitatively using a generalized substitution technique.[13-15] The power spectrum of the backscattered signal was

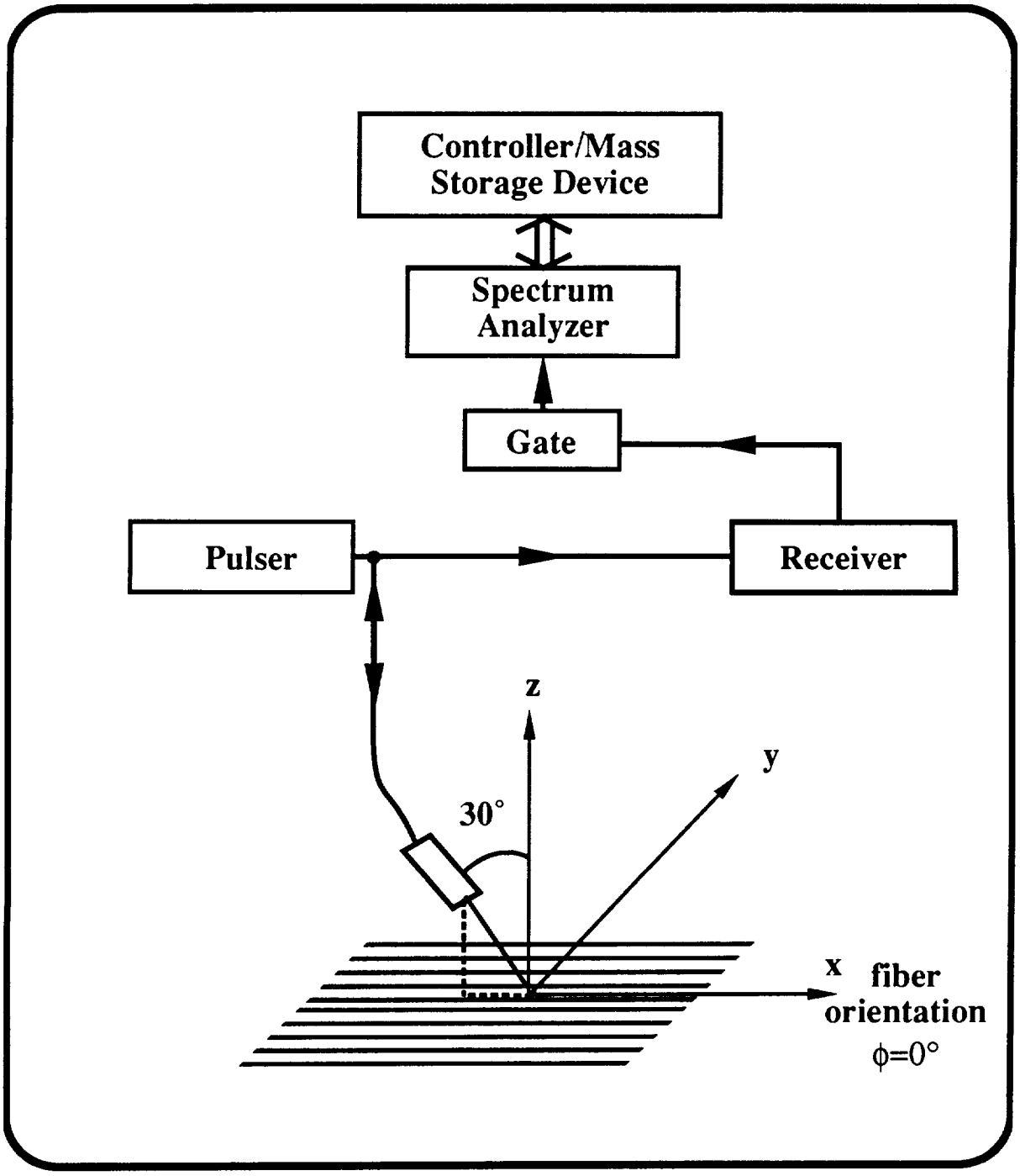

Figure 3: Block diagram of the polar backscatter data acquisition system.

obtained by gating a 9 μsec segment into an analog spectrum analyzer. This power spectrum was then normalized to the power spectrum obtained in a second (calibration) measurement in which the specimen was replaced by a nearly perfect (flat stainless steel) ultrasonic reflector, insonified at normal incidence. The result of this normalization, the backscatter transfer function, is independent of the electromechanical efficiency of the transducer and the properties of the system electronics. The backscatter transfer function is a relative measure of the backscattering efficiency as a function of frequency. The frequency average of the backscatter transfer function, termed the integrated backscatter, provides a useful index of backscatter efficiency over a finite bandwidth.[15,16] Frequency averaging over a broad bandwidth reduces the degrading influence of phase cancellation[15,17-20] and other interference effects which can compromise the results of backscatter measurements. The useful bandwidth chosen for all of the results presented in this Section of the Progress Report was over a range from 6 to 12 MHz.

RESULTS

Anisotropy of Polar Backscatter

Results of measurements performed with the bleeder cloth impressions intact were compared with the corresponding results obtained after their complete removal by surface grinding. Figure 4 displays the integrated backscatter difference in a graphite/epoxy laminate for measurements taken in a "porous" and pore-free region. With bleeder cloth impressions removed, the integrated backscatter difference was 16 dB for a pore-free region and 3 dB for a region containing approximately 3.4% volume fraction of "porosity". In contrast, for measurements made on the same sample prior to the complete removal of the bleeder cloth impression, the integrated backscatter difference was 5.5 dB for a pore-free region and 5.6 dB for the region containing approximately 3.4% "porosity". Thus the measurements carried out after the bleeder cloth impressions were completely removed displayed a large difference (12 dB) between the "porous" and pore-free regions. In contrast, measurements carried out with the bleeder cloth impressions intact yielded virtually identical results in the "porous" and pore-free regions. These results indicate that the presence of bleeder cloth impressions remaining after the cure process can contribute significantly to the received backscatter signal, masking the anisotropy of polar backscatter.

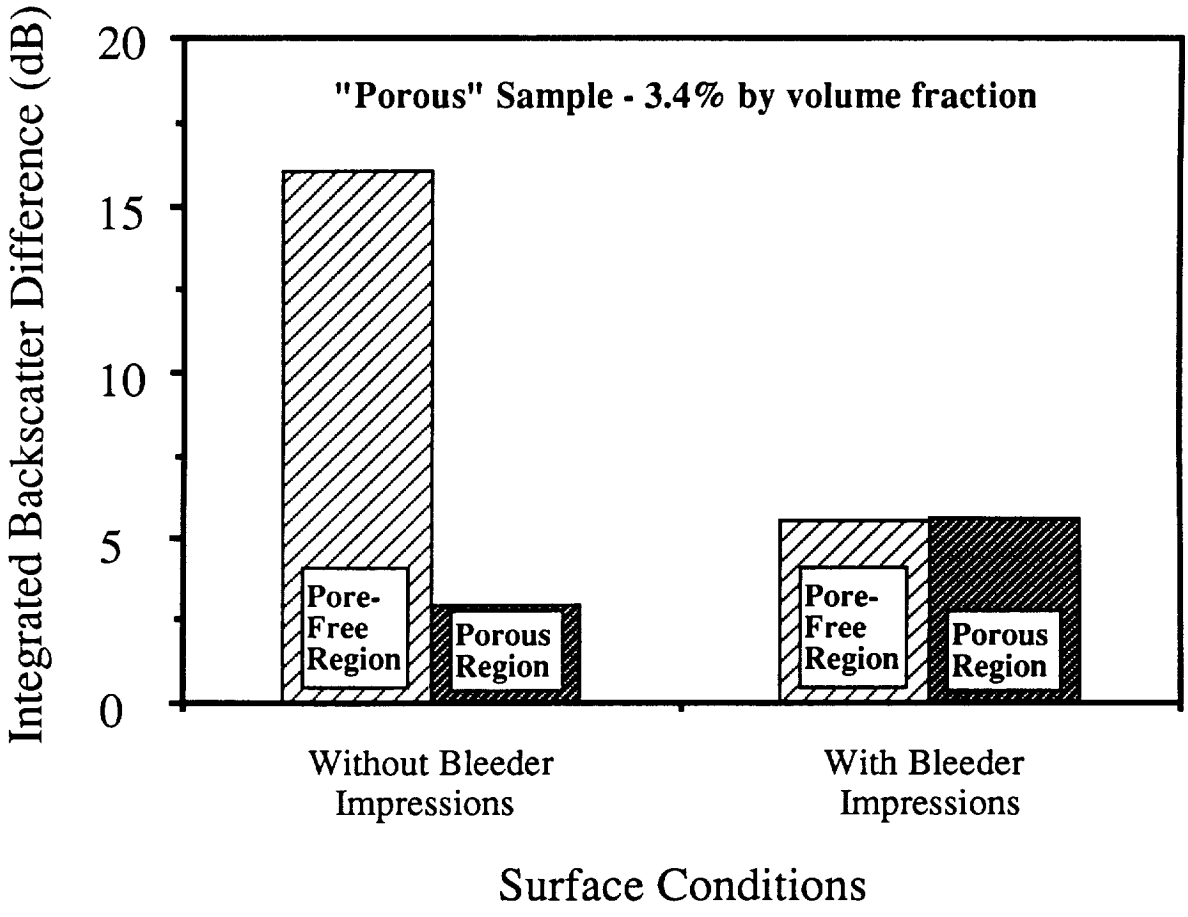

Figure 4: Influence of surface conditions on the integrated backscatter difference for measurements taken in a "porous" (3.4% by volume fracton) and a pore-free graphite/epoxy laminate.

Systematic Reduction of Bleeder Cloth Effects

In order to delineate the relative contributions of undesirable scattering from bleeder cloth impressions on the top and bottom surfaces, three sets of anisotropy scans were performed on the same region of a pore-free uniaxial graphite/epoxy composite. Prior to Scan 1, one side of the sample had been surface ground to remove the bleeder cloth impression and the other side had the bleeder cloth impression left intact. Insonification was from the side with the bleeder cloth impression. Scan 2 was performed with the composite in the same state as for Scan 1 except that the sample was flipped over and insonified from the side from which we had completely removed the bleeder cloth impression. Prior to Scan 3, we surface ground the second side and then repeated the measurement.

Scans were carried out at a polar angle of 30° and azimuthal angles varying from -110° to +110° in 2° increments. Each sample was scanned on a 4 by 4 grid in 2.5 mm steps and the acquired frequency spectra were averaged to reduce the effects of spatial variations. Integrated polar backscatter is plotted as a function of azimuthal angle for each of the scans in Figure 5. As illustrated previously (see Figure 1) the polar backscatter signal is expected to be the largest for azimuthal angles where the insonifying beam is perpendicular to the fiber axes ($\phi = \pm 90°$) and smallest for angles of insonification approximately parallel to the fiber axis ($\phi = 0°$). Although the results from Scan 1 of Figure 5 display the expected maxima for $\phi = \pm 90°$, there is an unexpected peak at $\phi = 0°$ and a substantial backscattered signal for azimuthal angles between -90° and +90°. The relative contributions of these unexpected results are significantly diminished in Scan 2 (bleeder cloth impression on opposite side) relative to those in Scan 1 (bleeder cloth impression on insonified side). It is interesting to note that the unexpected peak at $\phi = 0°$ is still evident in Scan 2. Inspection of the data trace from Scan 3 for which the bleeder cloth impression had been removed from both sides reveals the expected results for a uniaxial composite laminate. That is, for angles of insonification perpendicular to the fiber orientation the polar backscatter displays peaks that are significantly stronger than signals received for nonperpendicular angles, and the minimum occurs for insonification parallel to the fibers.

Quantitative Imaging

Practical applications of the methods of polar backscatter to characterize porosity require the generation of two dimensional images to map suspected regions of porosity. Figure 6 displays the results obtained from a quantitative mapping of a composite containing a localized region of "porosity", 2% by volume fraction. A raster scan was

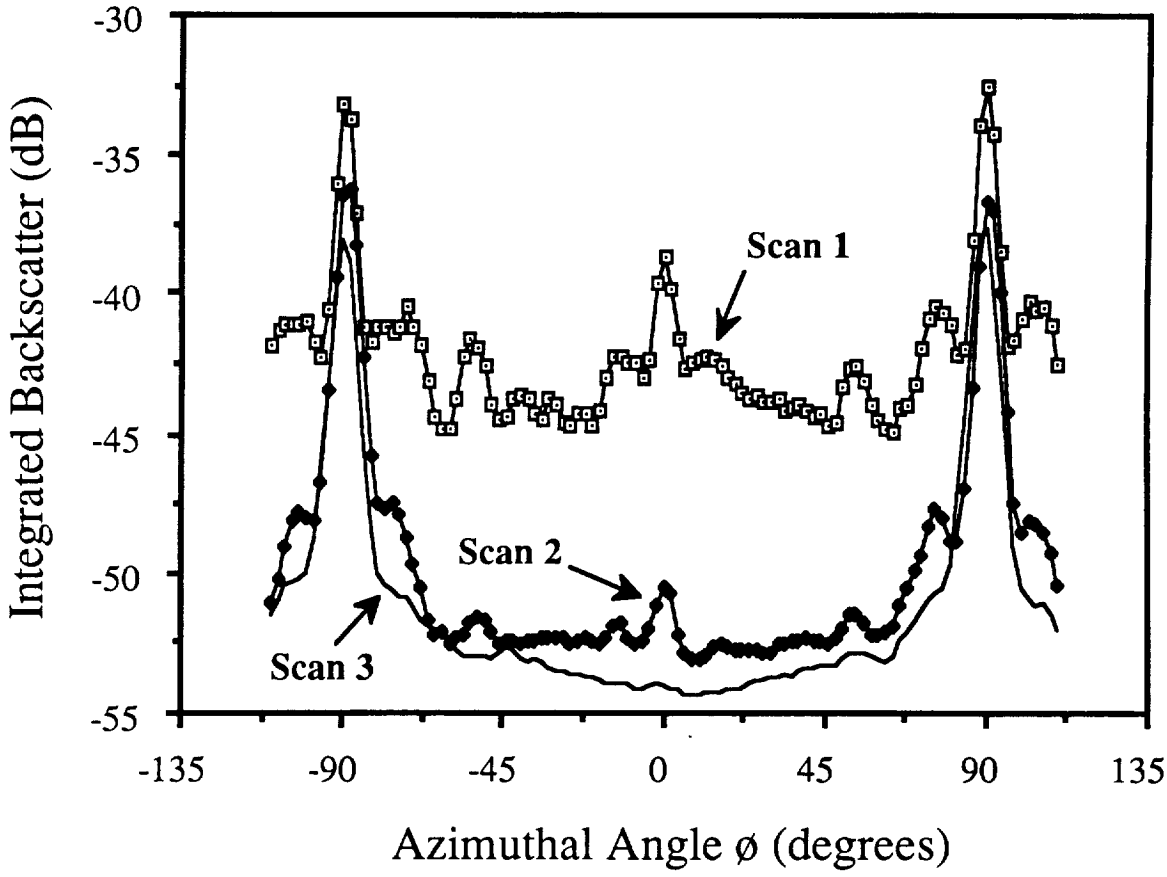

Figure 5: Anisotropy scans displaying results for 3 surface conditions. In Scans 1 and 2 one side of the composite had been surface ground. The side with the bleeder cloth impression intact was insonified in Scan 1. The side with the bleeder cloth impression removed was insonified in Scan 2. For Scan 3, both sides had been surface ground.

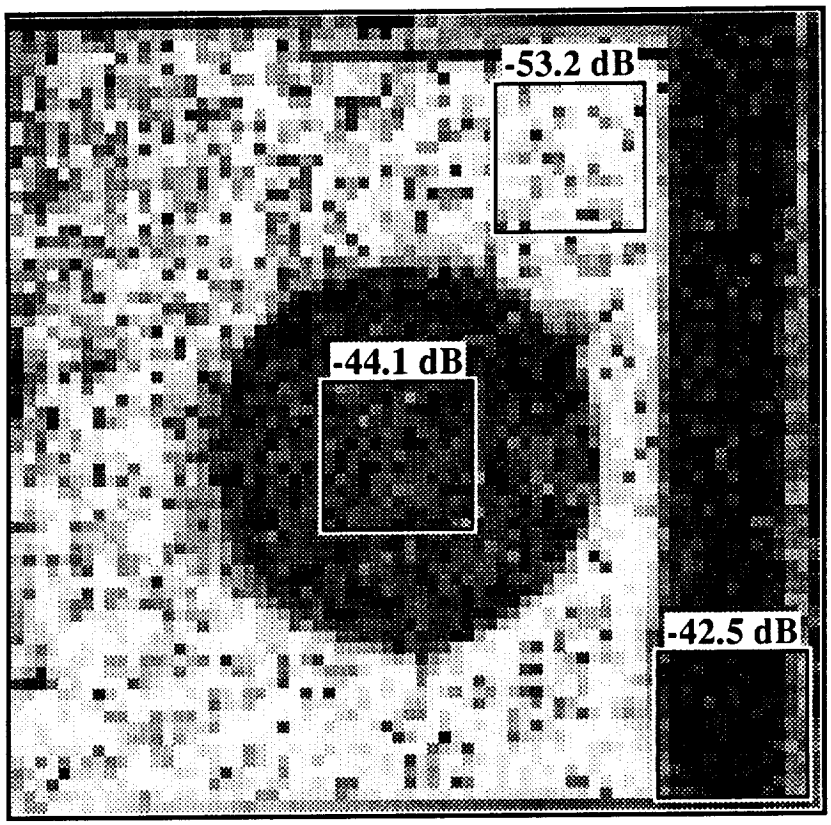

Figure 6: A quantitative mapping (ø = 0°) of a composite containing a localized region of "porosity", 2% by volume fraction.

performed over a square grid using a step size of 1.5 mm. The azimuthal angle of insonification was fixed parallel to the fiber orientation ($\phi = 0°$). The value (in dB) shown for each region is the mean of 169 sites. The circular region in the center of the scan in Figure 6 corresponds to the region of "porosity". The region exhibits an average value of integrated backscatter 44.1 dB below that from a stainless steel (reference) plate. In contrast, typical integrated backscatter values in the pore-free regions average 53.2 dB below that from a stainless steel plate. As an illustration of the potentially confounding role of bleeder cloth impressions, a 1 inch wide vertical strip at the right of the image corresponds to a region where the depth of the grinding to remove the bleeder cloth impression was limited so that a faint impression remained. Even this relatively faint impression on the insonified surface was sufficient to produce a value of integrated backscatter of -42.5 dB relative to that of a stainless steel plate. This value is 1.6 dB larger than that (-44.1 dB) characteristic of the zone of "porosity".

DISCUSSION

Considerable progress has been reported in recent experimental and theoretical investigations of the potential role of polar backscatter in detecting and characterizing porosity.[7-10] Nevertheless, practical implementation of this approach will be feasible only after the confounding effects of surface conditions can be reliably eliminated from the measured signals. The results of this investigation indicate that the presence of the bleeder cloth impressions substantially influences the degree of anisotropy. Furthermore, for relatively thin samples in which selective time gating is not feasible, not only the state of the insonified surface but also the state of the back surface influences the received signal. Some additional effects pertinent to the study of relatively thin laminates have been investigated by other authors.[11] Although removing these impressions by surface grinding provided a satisfactory approach for this laboratory investigation, an easily reversible surface treatment to minimize scattering from bleeder cloth impressions and similar surface features will be required in practical applications.

III. MATERIALS CHARACTERIZATION USING PHASE-INSENSITIVE AND PHASE-SENSITIVE IMAGING

As an approach to developing improved methods for materials characterization, phase-insensitively and phase-sensitively derived experimental values of the average scattered power were compared for measurements of the same scattered field due to a distribution of glass-bead scatterers embedded in gelatin, measured with a two-dimensional pseudo-array. The effects of introducing phase-distorting media (a

polyethylene wedge or grooved plate) in front of the receiving array on the phase-insensitively and phase-sensitively derived parameters were investigated under conditions of planar, spherical, and "correlation" focusing.

The experimental arrangement used to measure the scattered ultrasonic field was similar to that used previously at this Laboratory.[21,22] A 0.5-inch diameter, 5 MHz center-frequency, 4-inch (101 mm) focal length, broadband piezoelectric transmitting transducer was focused at the surface of a glass-bead phantom. A two-dimensional pseudo-array receiver arrangement was achieved by translating a planar 5 MHz center-frequency broadband piezoelectric transducer, apodized (with a Styrofoam plate) to 1 mm in diameter, in a 13 X 13 grid pattern with 1 mm separation between adjacent grid positions. The receiving pseudo-array was centered at a scattering angle of 160° ("back-scatter") with respect to the direction of the transmitted ultrasonic beam. The ultrasonic rf signal measured at each position of the receiver array was amplified, electronically gated, signal averaged, and digitized at a sampling rate of 100 megasamples/sec. The digitized signal-averaged rf signal obtained at each array position was stored for further analysis. Movement of the apodized receiving transducer to form the two-dimensional pseudo-array was controlled by a microcomputer.

The glass-bead scattering phantom consisted of a distribution of solid glass beads ranging from 63 to 158 μm in diameter embedded in gelatin. The concentration of glass beads was approximately 60 beads/mm^3. The phantom was immersed in a water bath and located approximately 101 mm away from both the transmitting transducer and the plane of the two-dimensional pseudo-array receiver.

The effects of introducing phase-distorting media in front of the receiving array on the phase-insensitively and phase-sensitively derived average power values were investigated. The phase-distorting media used in this investigation consisted of a polyethylene wedge or grooved plate. The polyethylene wedge was a 38.1 mm by 38.1 mm square with a thickness of 5.44 mm at one edge and tapering linearly to a thickness of 1.27 mm at the opposite edge. The polyethylene grooved plate was a 38.1 mm by 38.1 mm square plate whose thickness was 3.15 mm except for two grooves, each of 3.18 mm in width, milled adjacently across the center of the plate. The depths of the grooves were 0.46 mm and 0.79 mm. Each of the phase-distorting plates were placed, in turn, approximately 3 mm in front of the two-dimensional pseudo-array. Care was taken to align the plates parallel to the plane of the two-dimensional pseudo-array.

The "backscattered" field investigated was that field contained in a 4.0 μsec gated region which included the front surface and the region immediately behind the front surface of the glass-bead phantom. The signal loss (attenuation plus reflection losses) due to

the polyethylene phase-distorting media were removed by compensating for the measured losses through polyethylene. The "backscattered" ultrasonic field was measured for 10 statistically independent sites in the glass-bead phantom for each of the phase-distorting media introduced (none, wedged, or grooved). Results from each independent phantom site were averaged and the mean value and its corresponding standard error are reported.

Several focusing schemes were applied to the ultrasonic data acquired by the two-dimensional pseudo-array. The focusing schemes employed were: planar focusing, spherical focusing, and "correlation" focusing. In planar focusing, no time shifts were applied to the recorded rf waveforms obtained at each position in the pseudo-array. Thus, the data represent what a planar receiver would measure. Spherical focusing of the array was achieved by applying the appropriate time delays to the rf waveforms recorded at each position of the pseudo-array in order to focus at a point. These time delays were determined by calculating the time-of-flight of an ultrasonic wave from each position in the array to a point located a distance of 101.6 mm (distance between pseudo-array and phantom) from the center position of the array on a line perpendicular to the the plane of the array. The "correlation" focusing method employed is based in part on techniques introduced previously by others.[23, 24] The time shift applied to the rf waveform recorded at each position in the pseudo-array was determined by maximizing the cross-correlation between the waveform recorded at a given position and the waveform recorded at the center position for a finite range of shifts tested. In the case of no intervening phase-distorting medium, a 1.0 μsec range of shifts (±0.5 μsec) was tested. For the cases with phase-distorting media, a 2.0 μsec range of shifts (±1.0 μsec) was tested. In all cases the increment per shift was 0.01 μsec.

Both phase-sensitive and phase-insensitive analyses were applied to the rf data collected with the two-dimensional pseudo-array. For phase-sensitive analysis the individual rf waveforms recorded at each of the array positions were focused as desired, summed, and normalized, thus producing a single rf waveform for the array. A region of interest was gated from the resultant waveform and the average power was determined. Phase-insensitive analysis was achieved by applying the desired focusing to the rf waveform obtained at a given array position, gating a region of interest, and then determining the average power for that array position. The average power value for each of the array positions were summed and normalized to give the phase-insensitive value for the array as a whole.

The values of the average power contained in a 4.0 μsec gated region of the scattered ultrasonic field, determined phase-sensitively and phase-insensitively for the

various phase-distorting intervening media and focusing schemes, are displayed in Figures 7a, 7b, and 7c. Figure 7a shows the phase-insensitively and phase-sensitively determined values of the average power for the three focusing schemes without a phase-distorting medium between the scattering phantom and the receiving pseudo-array. The phase-insensitively determined values are larger in magnitude than the phase-sensitively determined values and do not appear to depend significantly on focusing scheme used. Conversely, the phase-sensitively determined values appear to be very dependent on focusing scheme used. As illustrated in Figure 7a, the difference between the phase-insensitively and phase-sensitively determined values is the greatest for the planar-focused case (14.0 dB) and is smaller for the spherically-focused (5.6 dB) and "correlation"-focused (4.6 dB) cases.

Figure 7b shows the phase-insensitively and phase-sensitively determined values of the average power for the three focusing schemes when the wedge-shaped phase-distortion plate was positioned between the scattering phantom and the receiving pseudo-array. (Compensation for the effects of the signal loss due to the attenuation and insertion loss of the polyethylene wedge phase-distortion plate was carried out prior to the generation of Figure 7b.) As in Figure 7a, the phase-insensitively determined values do not depend strongly on the focusing technique employed whereas the phase-sensitively determined values do. The phase-insensitive values are larger in magnitude than those for phase-sensitive detection, with a 13.0 dB difference for planar focused, 12.6 dB difference for spherically focused, and 4.4 dB difference for "correlation" focused. Contrasting this figure with Figure 7a reveals that the magnitude of the spherically-focused phase-sensitively determined value is not as large as that in the case of no phase-distorting intervening medium. This may be due to the fact that the phase-distorting wedge distorts the phase-fronts of the scattered field but the focusing employed was appropriate for an undistorted field emanating from a point 101.6 mm away. Thus the focusing shifts employed to the rf data do not focus the data properly, and hence significant phase-cancellation effects across the array may be present.

The values of the phase-insensitively and phase-sensitively determined average power for the case of the intervening grooved polyethylene phase-distortion plate are shown in Figure 7c. (Here again the signal-loss effects of the phase-distortion plate have been removed.) As above, the phase-insensitively derived values are larger in magnitude than the phase-sensitively derived values for all focusing techniques employed, and the phase-insensitively determined values do not depend strongly on focusing technique used whereas the phase-sensitively derived values do. The difference between the phase-insensitively derived values and the phase-sensitively derived values show a dependence

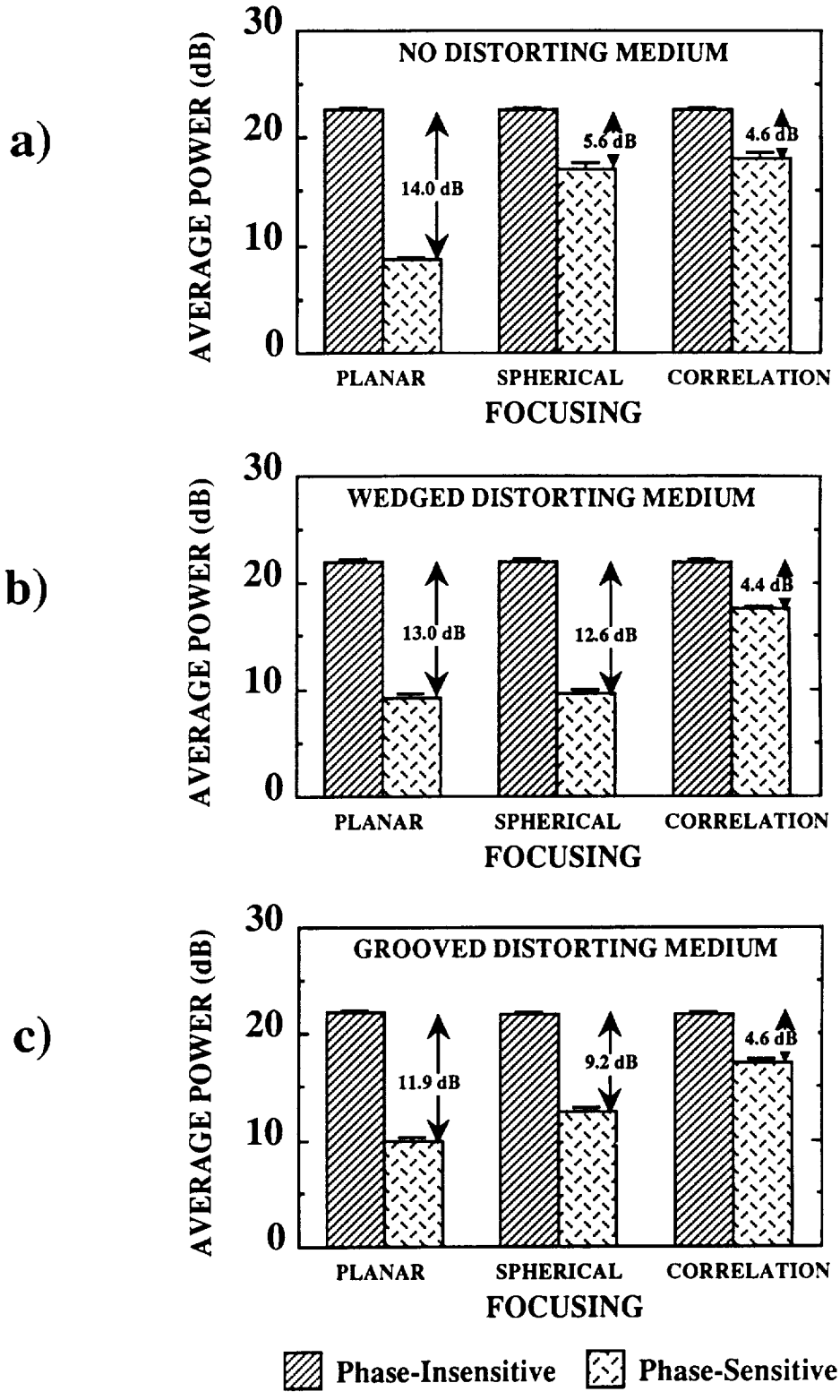

Figure 7: Average power in 4.0 μsec gated region for various focusing schemes and intervening phase-distorting media.

upon focusing scheme used much in the same manner as that discussed for the wedge phase-distortion plate above. The differences in this case are 11.9 dB for the planar-focused case, 9.2 dB for the spherically-focused case, and 4.6 dB for the "correlation"-focused case.

References

1. Y. Bar-Cohen and R.L. Crane, "Acoustic-Backscattering Imaging of Subcritical Flaws in Composites," *Materials Evaluation*, vol. 40, pp. 970-975, 1982.
2. Lewis J. Thomas III, Eric I. Madaras, and J.G. Miller, "Two-Dimensional Imaging of Selected Ply Orientations in Quasi-Isotropic Composite Laminates Using Polar Backscattering," *Proc. IEEE Ultrasonics Symposium*, vol. 82 CH 1823-4, pp. 965-970, (1982).
3. D.E. Yuhas, C.L. Vorres, and Ronald A. Roberts, "Variations in Ultrasonic Backscatter Attributed to Porosity," *Review of Progress in Quantitative NDE*, vol. 5, pp. 1275-1284, Plenum Press, New York, 1985.
4. Earl D. Blodgett, Lewis J. Thomas III, and J.G. Miller, "Effects of Porosity on Polar Backscatter From Fiber Reinforced Composites," *Review of Progress in Quantitative Nondestructive Evaluation*, vol. 5B, pp. 1267-1274, (1986).
5. Earl D. Blodgett, S.M. Freeman, and J.G. Miller, "Correlation of Ultrasonic Polar Backscatter With the Deply Technique for Assessment of Impact Damage in Composite Laminates," *Review of Progress in Quantitative Nondestructive Evaluation*, vol. 5B, pp. 1227-1238, (1986).
6. S.M. Handley, M.S. Hughes, J.G. Miller, and E.I. Madaras, "Characterization of Porosity in Graphite Epoxy Composite Laminates With Polar Backscatter and Frequency Dependent Attenuation," *IEEE Ultrasonics Symposium*, vol. 87CH2492-7, pp. 827-830, (1987).
7. Ronald A. Roberts, "Porosity Characterization in Fiber-Reinforced Composites by Use of Ultrasonic Backscatter," *Review of Progress in Quantitative NDE*, vol. 6B, pp. 1419-1156, Plenum Press, New York, 1987.
8. J. Qu and J.D. Achenbach, "Analytical Treatment of Polar Backscattering From Porous Composites," *Review of Progress in Quantitative NDE*, vol. 6B, pp. 1137-1146, Plenum Press, New York, 1987.
9. Ronald A. Roberts, "Characterization of Porosity in Continuous Fiber-Reinforced Composites with Ultrasonic Backscatter," *Review of Progress in Quantitative NDE*, vol. 7B, pp. 1053-1062, Plenum Press, New York, 1988.

10. J. Qu and J.D. Achenbach, "Backscatter From Porosity in Cross-Ply Composites," *Review of Progress in Quantitative Nondestructive Evaluation*, vol. 7B, pp. 1029-1036, 1988.

11. T. Ohyoshi and J.D. Achenbach, "Effect of Bottom-Surface Reflections on Backscatter From Porosity in a Composite Layer," *Review of Progress in Quantitative Nondestructive Evaluation*, vol. 7B, pp. 1045-1052, 1988.

12. Yoseph Bar-Cohen, *Nondestructive Characterization of Defects in Multilayered Media Using Ultrasonic Backscattering,* McDonnell-Douglas Corp., 1987. Douglas Paper 7781. Unpublished.

13. M. O'Donnell, J.W. Mimbs, and J.G. Miller, "The Relationship Between Collagen and Ultrasonic Backscatter in Myocardial Tissue," *J. Acoust. Soc. Am.*, vol. 69, pp. 580-588, (1981).

14. M. O'Donnell and J.G. Miller, "Quantitative Broadband Ultrasonic Backscatter: An Approach to Non-Destructive Evaluation in Acoustically Inhomogeneous Materials," *J. Appl. Phys.*, vol. 52, pp. 1056-1065, (1981).

15. J.G. Miller, J.E. Perez, Jack G. Mottley, Eric I. Madaras, Patrick H. Johnston, Earl D. Blodgett, Lewis J. Thomas III, and B.E. Sobel, "Myocardial Tissue Characterization: An Approach Based on Quantitative Backscatter and Attenuation," *Proc. IEEE Ultrasonics Symposium*, vol. 83 CH 1947-1, pp. 782-793, (1983).

16. M. O'Donnell, D. Bauwens, J.W. Mimbs, and J.G. Miller, "Broadband Integrated Backscatter: An Approach to Spatially Localized Tissue Characterization In Vivo," *Proc. IEEE Ultrasonics Symposium*, vol. 79 CH 1482-9, pp. 175-178, (1979).

17. J.S. Heyman, "Phase Insensitive Acoustoelectric Transducers," *J. Acoust. Soc. Am.*, vol. 64, pp. 243-249, 1978.

18. L.J. Busse and J.G. Miller, "Detection of Spatially Nonuniform Ultrasonic Radiation with Phase Sensitive (Piezoelectric) and Phase Insensitive (Acoustoelectric) Receivers," *J. Acoust. Soc. Am.*, vol. 70, pp. 1377-1386, (1981).

19. L.J. Busse and J.G. Miller, "A Comparison of Finite Aperture Phase Sensitive and Phase Insensitive Detection in the Near Field of Inhomogeneous Material," *Proc. IEEE Ultrasonics Symposium*, vol. 81 CH 1689-9, pp. 617-626, (1981).

20. L.J. Busse and J.G. Miller, "Response Characteristics of a Finite Aperture, Phase Insensitive Ultrasonic Receiver Based Upon the Acoustoelectric Effect," *J. Acoust. Soc. Am.*, vol. 70, pp. 1370-1376, (1981).

21. Patrick H. Johnston and J.G. Miller, "Phase-Insensitive Detection for Measurement of Backscattered Ultrasound," *IEEE Trans. Ultrasonics, Ferroelectrics, and Frequency Control*, vol. UFFC-33, pp. 713-721, (1986).

22. Patrick H. Johnston, *Phase-Insensitive Detection and the Method of Moments for Ultrasonic Tissue Characterization,* Washington University, St. Louis, Mo., August, 1985. Ph.D. Thesis.

23. K. V. Gurumurthy, *Adaptive Pulse-Echo Imaging for Quantitative Ultrasonic Tissue Characterization*, Washington University, St. Louis, MO, August 1981. Ph.D. Thesis

24. C. Nelson Dorny, "A Self-Survey Technique for Self-Cohering of Antenna Systems," *IEEE Trans. on Antennas and Propagation*, vol. AP-26, pp. 877-881, November 1978.